

# Assessing the impact of observations on a local numerical fog prediction system

S. Rémy\* and T. Bergot

CNRM/GAME, 42 Av. Coriolis, 31057 Toulouse Cedex 1, France

**ABSTRACT:** As poor visibility conditions have great influence on air traffic, a need exists for accurate, updated fog and low-cloud forecasts. COBEL–ISBA, a boundary-layer one-dimensional numerical model, has been developed for the very short-term forecasting of fog and low clouds. This forecasting system assimilates the information from a local observation system designed to provide details on the state of the surface boundary layer, as well as that of the fog and low-cloud layers.

This article aims to assess the influence of each component of the observation system on the initial conditions and low-visibility forecasts. The objective is to obtain a quantitative assessment of the impact on numerical fog forecasts of using a reduced (for smaller-sized airports) or enhanced (using a sodar) set of observations. We first used simulated observations, and focused on modelling the atmosphere before fog formation and then on simulating the life-cycle of fog and low clouds. Within this framework, we also estimated the impact of using a sodar to estimate the thickness of the cloud layer. We showed that the radiative flux observations were the most important of all in cloudy conditions, and that the measurement mast did not have to be higher than 10 m. Using either a sodar or radiative flux to estimate the optical thickness of a cloud layer gave the same scores. Using both of them together did not significantly improve the forecast. Simulations with real observations over a winter of simulations confirmed these findings. Copyright © 2009 Royal Meteorological Society

**KEY WORDS** data assimilation; 1D model; local observations; PBL; airports; low-visibility conditions; fog

Received 24 October 2008; Revised 26 February 2009; Accepted 29 April 2009

## 1. Introduction

Low-visibility conditions often cause problems for many international airports. Such conditions may reduce the landing/takeoff traffic by a factor of two, leading to delays or even cancellations of flights. This is why accurate forecasts of these conditions have become an important issue. Each airport defines a set of visibility and ceiling thresholds below which safety procedures, called low-visibility procedures (LVP), are applied. At Paris–Charles De Gaulle airport, the threshold values are set at 600 m for visibility and 60 m for the ceiling.

Various approaches are employed to forecast low-visibility conditions. Three-dimensional (3D) models with detailed microphysics have been tested for airports situated in regions with complex orography (Müller *et al.*, 2005; Capon *et al.*, 2007). For airports located in flat terrain, one-dimensional (1D) models are suitable for the nowcasting of radiation fog events (Bergot and Guédalia, 1994(a,b)). 1D ensemble methods have also been tried (Müller *et al.*, 2007; Roquelaure and Bergot, 2008). 1D models are currently used in real time to forecast fog at local scales (Clark, 2002, 2006; Herzegh *et al.*, 2003). The 1D boundary-layer model COuche Brouillard Eau Liquide (COBEL), coupled with the land-surface scheme

Interface Sol Biosphère Atmosphère (ISBA), as documented in Bergot *et al.* (2005), has been in operational use since 2005 at Paris–Charles de Gaulle airport in France to provide estimated times for the onset and lifting of LVP conditions. The model is also being installed over the Paris–Orly and Lyon–Saint Exupéry airports in France. To be able to forecast radiative fog events adequately, it possesses a high vertical resolution: 30 levels between 0.5 and 1360 m, with 20 levels below 200 m. ISBA is run with 7 levels in the ground, from 1 mm to 1.7 m below the surface. COBEL–ISBA is run at one-hour intervals and provides up to eight hours of LVP forecasts. The inputs of the model are the initial conditions and mesoscale forcings. In this article, we will focus on the latter. Mesoscale forcings (i.e. geostrophic wind, horizontal advection and cloud cover above the model column) are given by the Numerical Weather Prediction (NWP) model Aire Limitée Adaptation Dynamique Développement International (ALADIN, <http://www.cnrm.meteo.fr/aladin>). The initial conditions are given by a two-step assimilation scheme, using local observations (Bergot *et al.*, 2005). The observation system used at Paris–Charles de Gaulle airport is designed to provide up-to-date information on the state of the surface boundary-layer temperature and moisture, as well as on the microphysical properties of fog and low clouds. It includes the following.

- A weather station that provides 2 m temperature and humidity, visibility and ceiling.

\*Correspondence to: S. Rémy, CNRM/GAME, 42 Av. Coriolis, 31057 Toulouse Cedex 1, France. E-mail: samuel.remy@meteo.fr

- A measurement mast that gives temperature and humidity observations at 1, 5, 10 and 30 m.
- Radiative fluxes (short-wave and long-wave) at 2 and 45 m.
- Soil temperature and water content at the surface, -10, -20, -30 and -40 cm.

The assimilation system uses information from a first guess (i.e. a previous short-term COBEL-ISBA forecast), local observations and profiles from the ALADIN NWP model to generate a best linear unbiased estimator (BLUE) for the initial conditions of temperature and specific humidity. As the dimension of the system is low, matrices can be explicitly inverted and there is no need for a variational algorithm. When a layer of cloud is detected, an additional step uses a minimization algorithm together with measurement of radiative fluxes at the ground and at 45 m to estimate cloud thickness. The radiation scheme of COBEL is used to compute the modelled radiative fluxes at 2 and 45 m, using different initial thicknesses of the fog layer. The best estimate of the initial fog thickness is the one that minimizes the error between modelled and observed radiative fluxes (see Bergot *et al.*, 2005 for more details). The relative humidity profile is then modified within the saturated layer. The soil temperature and water-content profiles used to initialize ISBA are obtained directly by interpolation of soil measurements.

The question now is whether such a forecasting system can be applied for regional airports, which are more numerous than the international ones. In considering this, we also need to take into account the fact that these airports often lack sufficient financial support to implement a large-scale observation system equivalent to the one installed at Paris-Charles de Gaulle airport. It is therefore interesting to evaluate the importance of each component of the observation system, and its impact on the quality of the LVP forecasts. Bergot *et al.* (2005) have shown that forecasts with local observations have a significantly higher skill compared with those computed without the use of local information. The aim of this study is to refine this diagnosis, i.e. to assess the behaviour of the assimilation-forecast COBEL-ISBA numerical system when fewer inputs are used while comparing it with a reference observation system, the one at Paris-Charles de Gaulle. We also estimate the effectiveness of additional measurements such as those provided by a sodar, which enables us to estimate the height of the inversion layer (i.e. the layer in which temperature increases with altitude) that lies at the top of the fog (Cheung, 1991; Foken *et al.*, 1997; Yushkov and Kouznetsova, 2008).

In estimating the significance of each component of the observation system, we must distinguish between the formation of fog (clear-sky initialization) and its dissipation (low-cloud initialization), as different components of the assimilation system are used in the two cases. For the initialization in clear-sky conditions, the observations from the mast, the soil and the surface weather station are used. When low clouds are present at the initialization time, observations of radiative fluxes are also used in order to estimate the fog or low-cloud thickness. Also,

depending on the estimated height of the fog, the observations from the measurement mast will be partially or entirely discarded because modifications are made to the initial humidity profiles to adjust to a saturated atmosphere within the cloudy layer. Under such conditions, it is possible to study how accurately the assimilation scheme assesses the thickness of the cloud layer, and also the impact of the components of the observation system on the timing of the onset and lifting of fog and low clouds.

The framework of this study is outlined in section 2. Two sets of simulated observations were created: one with mostly clear-sky conditions at the initialization, to study the formation of fog, and the other with the frequent occurrence of fog and low clouds. Section 3 shows the results obtained from the first set of observations and section 4 shows those from the second set. Next, in section 5, we focus on results obtained from a system using real observations instead of simulated ones. Finally, in section 6 we summarize and discuss the possibility of using the COBEL-ISBA forecasting system for medium-sized airports.

## 2. Framework of the study: simulated observations

The Observing System Simulation Experiment (OSSE) is adequate to study the accuracy of an assimilation scheme (Huang *et al.*, 2007). It consists of generating pseudo-observations by adding perturbations to a reference model run. The pseudo-observations are then assimilated, and the initial state and forecast can be compared with the reference run. The advantages of this method are as follows.

- The perfect model hypothesis is true, thus fitting the hypothesis made in the BLUE assimilation algorithm. The errors in the initial conditions originate only in the observations and first-guess errors, which themselves originate from errors in the initial conditions propagated by the previous forecast. The lack of observations for certain parameters (e.g. the thickness or water content of a cloud layer) does not allow the assimilation scheme to entirely correct the errors of the first-guess field. The quality of initial conditions thus depends solely on the observations used and on the assimilation scheme.
- This framework allows observations to be simulated over the whole domain (the boundary layer for this study) or supplementary observations to be synthesized. Sodars can be used to provide the height of the inversion layer that lies just above the top of the fog layer. It is thus a good indicator of its thickness. With simulated observations, we can create observations from a perfect sodar that give the exact height of the fog layer top. This may be due to the interface between the soil and the atmosphere, which degraded the results close to the surface.
- Lastly, it is possible to create a large variety of observation sets that accommodate our needs for evaluation purposes.

A reference run is first carried out, which represents the hypothetically 'true' state of the atmosphere,  $x^t$ . The

simulated observations  $y_i^0$  are then computed by adding a perturbation  $v_i$  taken from a normal distribution of zero mean and standard deviation  $\sigma_i$ :

$$y_i^0 = x^t + v_i \quad v_i = \text{Normal}(0, \sigma_i).$$

The standard deviations of the errors in each component of the observation system are imposed, and these correspond to common observation errors. The error bias is assumed to be zero. The standard-deviation values are as follows: 0.3 K for atmospheric temperature on the mast, 0.1 g/kg for atmospheric specific humidity on the mast, 0.025 m<sup>3</sup>/m<sup>3</sup> and 0.3 K for soil water content and temperature respectively, and 5 W/m<sup>2</sup> for the radiative fluxes.

Profiles from the NWP ALADIN are also used by the assimilation system to complete the data for the upper levels. These pseudo-observations are synthesized in the same way, and the values used for the standard deviations of observation errors are 1.4 K for temperature and 0.5 g/kg for specific humidity, corresponding to estimated forecast errors.

The external forcings (geostrophic wind, horizontal advection and cloud cover above the model column) are considered to be constant during the reference simulation and for any further simulations. Geostrophic wind speed varies from 3 m/s close to the ground to 13 m/s at the top of the domain (i.e. 1360 m). The absence of cloud cover is imposed above the domain of COBEL–ISBA, while the horizontal advection of temperature and humidity is zero.

The model is run every hour over a 15 day period, giving rise to a total of 360 simulations.

### 3. Near-fog situation

In this section, as the results for temperature and specific humidity are mostly similar, humidity results are referred to where they are relevant.

#### 3.1. Presentation of the situation

Simulated observations corresponding to clear-sky and shallow-fog situations were produced. This observation set will be referred to as NEAR-FOG hereafter. 15 days of simulated observations were generated, during which no fog occurred for the first 10 nights. Shallow-fog situations developed for the remaining five nights. Their thicknesses did not exceed 10 m. 21 hours of LVP conditions were ‘observed’ for this situation. As mentioned, the skies above the model column were entirely clear, which ensured strong night-time cooling. Figure 1 shows the ‘true’ temperature at 1 m and corresponding liquid water path. Close to ground level, the daily highs lay in the 20–22°C range while the lows were around 8–9°C. Day and night relative humidity varied greatly from 30% to 100%, corresponding to typical conditions observed during winter over land.

The reference observation system was the one installed at Paris–Charles de Gaulle airport, which was introduced

above. Radiative flux observations are used only in the presence of fog or low clouds, which are not frequent for this case. We assumed that a weather station providing 2 m temperature and relative humidity, together with ceiling and visibility, was present. Three scenarios were investigated.

- MAST10: simulations using a 10 m mast (instead of 30 m for the reference), with temperature and relative humidity observations made at 1, 5 and 10 m (1, 5, 10 and 30 m for the reference). This height was chosen because the masts used to measure wind speed and direction at surface stations are 10 m high and could support the sensors to measure temperature and relative humidity.
- NOMAST: simulations using no mast. The only temperature and relative humidity observations were taken from the surface weather station in this case (at 2 m) and from the soil measurements.
- NOSOIL: simulations using no temperature or water-content measurements in the soil. A single temperature observation from the surface was used together with a first guess from ISBA to estimate these parameters below the surface. Above the ground, temperature and humidity at 2 m and from the observations of the 30 m mast were used.

#### 3.2. Simulations with the reference observation system: REF

The observation system used for these simulations was the one used at Paris–Charles De Gaulle airport. This experiment will be called ‘REF’. Figure 2 shows the root-mean-square error (RMSE) and the bias of the forecast temperature versus forecast time and altitude, together with the RMSE of the analyzed temperature versus simulation time for the 360 simulations of the NEAR-FOG situation.

The RMSE of analyzed temperature (Figure 2(a)) naturally increased with altitude, as the observations were concentrated in the lower part of the domain. Below 100 m, a weak diurnal cycle appeared, with lower RMSEs obtained during the day. For forecast temperature (Figure 2(b)), most of the degradation occurred during the first hour of simulation in the lower part of the domain. For forecast times greater than 2h, the forecast temperature RMSE no longer showed large differences between the lower and upper part of the domain, unlike the analyzed temperature. Also, above 100 m, the RMSE of forecast temperature was more or less constant with forecast time. The temperature bias (Figure 2(c)) was very small over the whole simulation domain at the initialization time. A cold bias appeared rapidly for the forecast temperature and increased regularly with the forecast time, with the maxima close to ground level.

#### 3.3. Simulations with a 10 m measurement mast: MAST10

The analysis was generated using temperature and humidity ‘observations’ from the weather station, 2 m above the

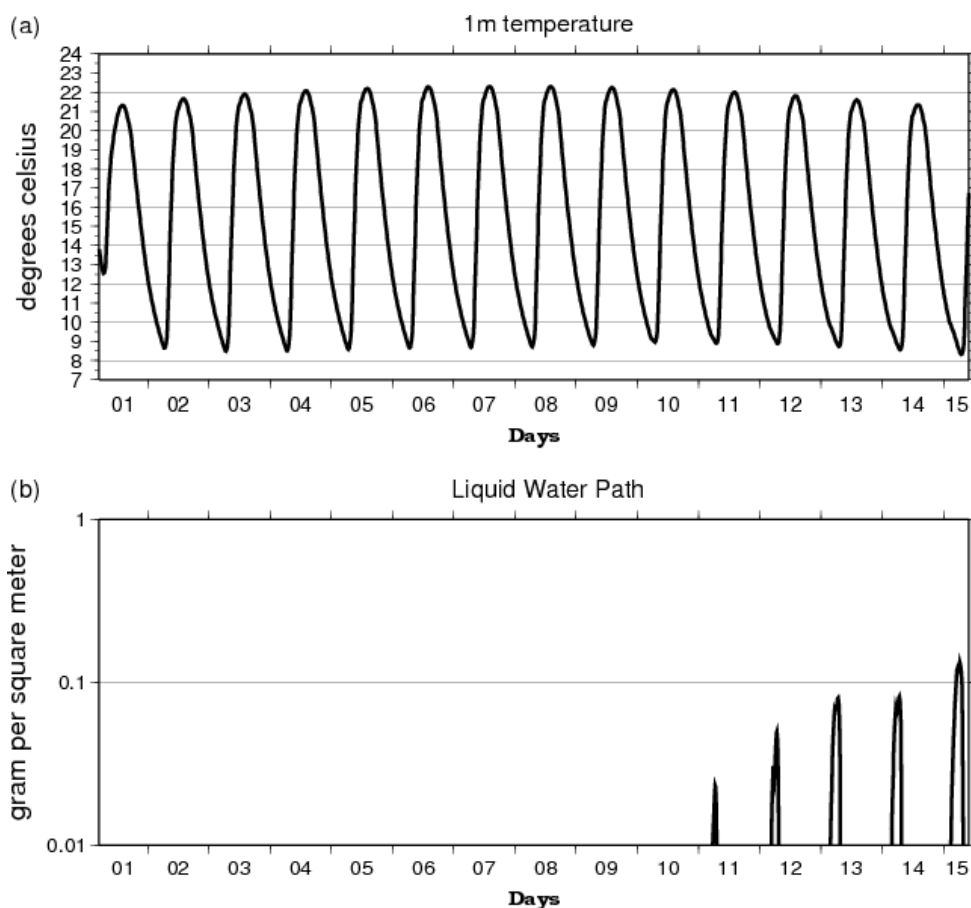


Figure 1. NEAR-FOG: 'Truth' for (a) 1 m temperature and (b) liquid water path.

ground, and a 10 m mast with measurements taken at 1, 5 and 10 m. Figure 3 shows the mean RMSE of the analyzed and forecast temperatures, for all 360 simulations of this experiment (MAST10), minus the mean RMSE of the REF experiment. The difference of absolute bias in temperature between the two experiments is also plotted.

The differences in analyzed temperature RMSE (Figure 3(a)) were positive almost everywhere, and more so between 20 and 100 m altitude during the night. During the day, from 0900 to 1700 UTC, the difference between REF and MAST10 was negligible for almost the whole simulation domain. This can be explained by the fact that in a neutral or slightly unstable atmosphere a temperature observation at 30 m does not provide much more information than a 10 m observation. However, this is no longer so when strong vertical temperature gradients occur, as in clear-sky nights.

This maximum of difference between the MAST10 and REF experiment above 10 m persisted during the forecast (Figure 3(b)), although it decreased with forecast time. Above that altitude, the degradation of MAST10 compared with REF was small and more-or-less constant with forecast time.

The initial temperature bias degradation (Figure 3(c)) resembled that of the RMSE, with degradation being maximum between 20 and 100 m of altitude and small above this.

In conclusion to the MAST10 experiment, it seems that the 30 m observation has little impact on temperature RMSE and bias close to the ground, which is most important for the forecast of radiation-fog events. This is probably due to the fact that the inversion layer always remained below 10 m during the NEAR-FOG case.

#### 3.4. Simulations with no mast: NOMAST

In this experiment, called NOMAST, no 'observations' from the mast were used. The only temperature and relative humidity observations available to improve the first guess were the ones coming from the surface weather station.

The lack of observations from the mast led to a degradation of the analysis (Figure 4(a)), which was more significant than for the MAST10 experiment (Figure 3(a)). A diurnal cycle appeared, as for MAST10; however, in contrast to MAST10, the analysis was degraded even for daytime runs. This shows that observations taken from the mast reveal extra information compared with the single 2 m observation used in the NOMAST experiment.

In comparison with MAST10, there was a considerable degradation in the RMSE of forecast temperature (Figure 4(b)). After three hours of forecast, the degradation relative to REF became very small close to the ground.

The bias was slightly less degraded for NOMAST (Figure 4(c)) than for MAST10 (Figure 3(c)), maybe

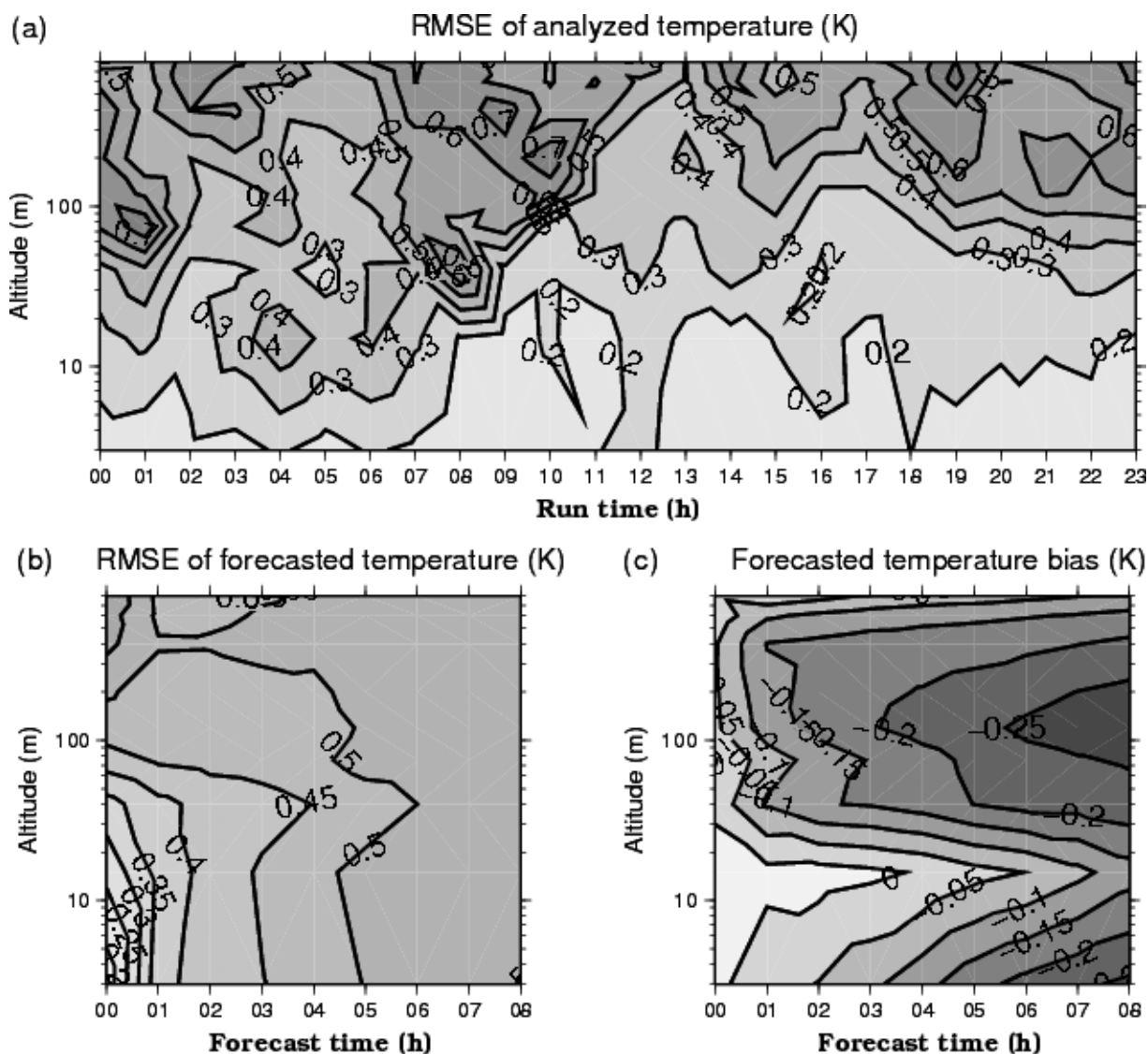


Figure 2. NEAR-FOG: RMSE of (a) analyzed and (b) forecast temperature versus simulation and forecast time respectively. (c) is the bias of forecast temperature, as a function of forecast time. Isolines are every 0.1 K for analyzed temperature and every 0.05 K for forecast temperature.

because the forecast was degraded during both day and night for NOMAST whereas it was only worse during the night for MAST10.

### 3.5. Simulations with no soil temperature or water-content observations: NOSOIL

For this experiment (called NOSOIL), we supposed that only one surface-temperature observation was available. The initial soil-temperature profile was computed by interpolation between the surface observation and a first guess coming from the previous run. For soil water content, the value given by the first guess was taken. The initial soil water content at the beginning of the experiment was kept constant for all ISBA levels, at 0.2 kg/kg.

The results of this experiment were dependent on the land-surface scheme used. The boundary-layer 1D model COBEL has been coupled with another land-surface scheme: NOAH (Chen *et al.*, 1997; Müller *et al.*, 2005). A 1D model intercomparison for the forecasting of fog

events (Bergot *et al.*, 2006) showed that COBEL–ISBA and COBEL–NOAH behaved differently. This confirms the impact of the land-surface scheme on the forecast of low-visibility conditions. In this section we try to assess the impact of observations in the soil when COBEL–ISBA is used.

The RMSE of both analyzed and forecast temperature (Figure 5(a) and 5(b)) showed little difference from the REF experiment. The initial soil-temperature and water-content profiles did not have a direct influence on the initial air-temperature profiles. They had an impact on the forecast and thus also an indirect influence on the initial profiles of air temperature and humidity through the first guess. However, in the lower atmosphere, the ‘observations’ taken from the weather station and the mast had much more weight in the computation of the initial conditions than the first guess, and the impact of the soil on the first guess is primarily at these levels. This explains why the initial atmospheric-temperature profiles were not affected by the lack of observations

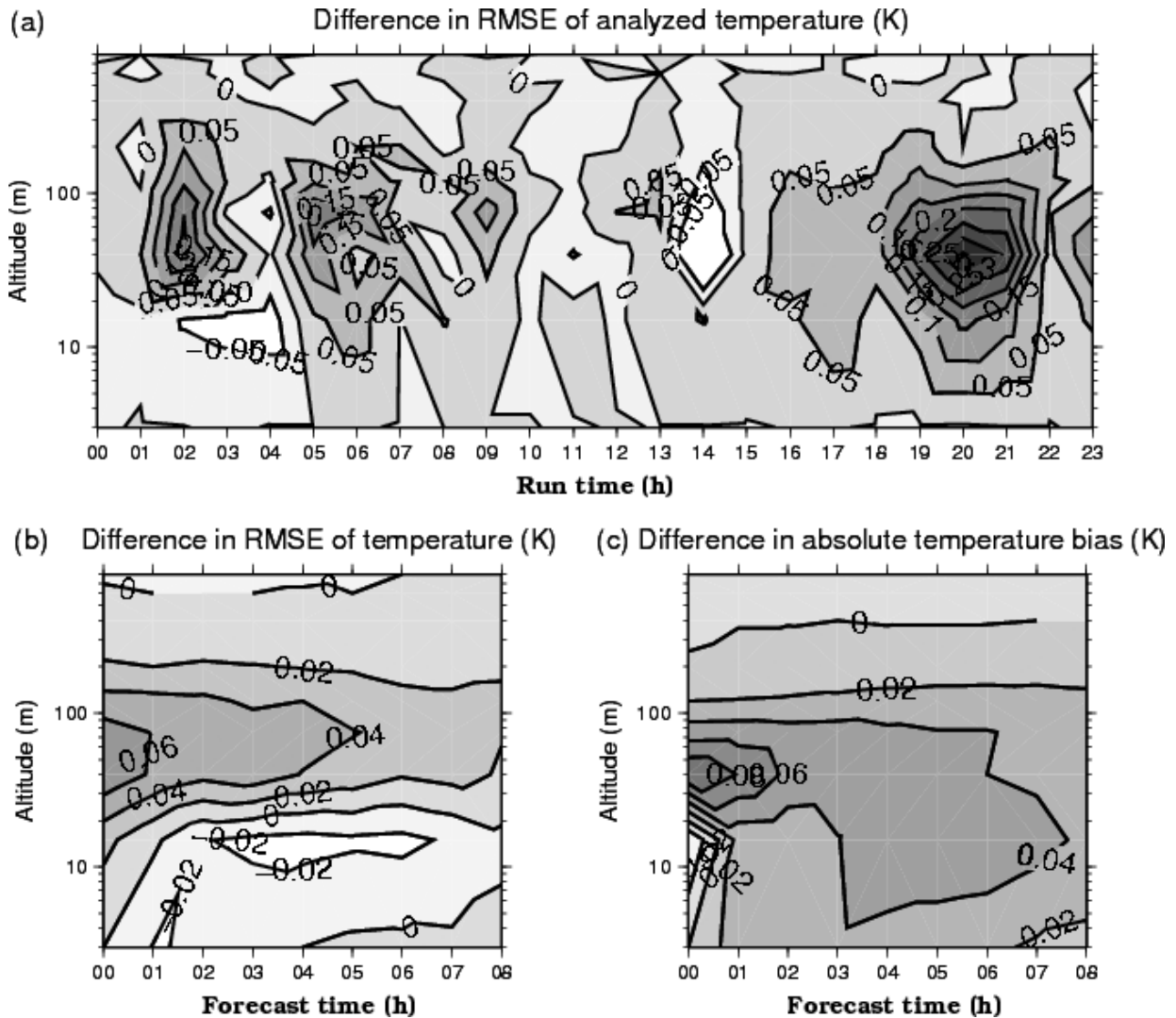


Figure 3. NEAR-FOG, MAST10 experiment: RMSE minus the RMSE of simulations using the reference observation system, (a) for analyzed temperature versus simulation time, (b) for forecast temperature versus forecast time. (c) is the absolute bias minus the absolute bias of simulations using the reference observation system, for forecast temperature versus forecast time. Isolines are every 0.05 K for analyzed temperature and every 0.02 K for forecast temperature. Positive values indicate a degradation of MAST10 compared with REF.

in the soil. As the soil temperature at the surface and the levels immediately below is strongly influenced by the observation, there was not much change in the RMSE of forecast temperature. The factor influencing the sensitivity to soil measurements was the water content. Its value had a great impact on the surface-cooling rate during the night and warming rate during the day. This brought a small fall in the RMSE of analyzed temperature after five to six hours of simulation.

The lack of soil water-content measurements led to a rise in temperature bias with forecast time, as compared with REF. The bias increase reached 0.1 K close to the ground after 3 h of forecast, and then increased slowly thereafter to 0.16 K after 7 h of simulation. The bias-degradation maximum was at the ground, as the degradation was driven by the surface. However, the degradation spread rapidly to the surface layer (below 20 m) and then to the boundary layer. The initial soil water content was greater than observed ( $0.2 \text{ m}^3/\text{m}^3$  against  $0.14$  'observed' at the surface to  $0.19$  at 1 m under the surface). The large

cold bias indicated that the weaker daytime warming brought about by a higher soil water content was not compensated by a smaller night-time cooling.

### 3.6. Beginning and end time of LVP conditions

Here, the error of the predicted onset time of LVP situations is evaluated. Table I shows the error of the predicted time of the onset of LVP conditions for the REF, MAST10, NOMAST and NOSOIL experiments. Simulations for which fog was present at initialization were discarded. The errors for the burn-off are not shown because they were relatively small, as the forecast and observed fog situations were both very shallow during NEAR-FOG. Both MAST10 and NOMAST showed a significant degradation of the forecast for the onset time of LVP conditions, while NOSOIL did not change the scores much. The number of large errors (arbitrarily defined as larger than 90 minutes in Table I) remained in the same range for the REF, NOMAST, MAST10 and NOSOIL experiments.

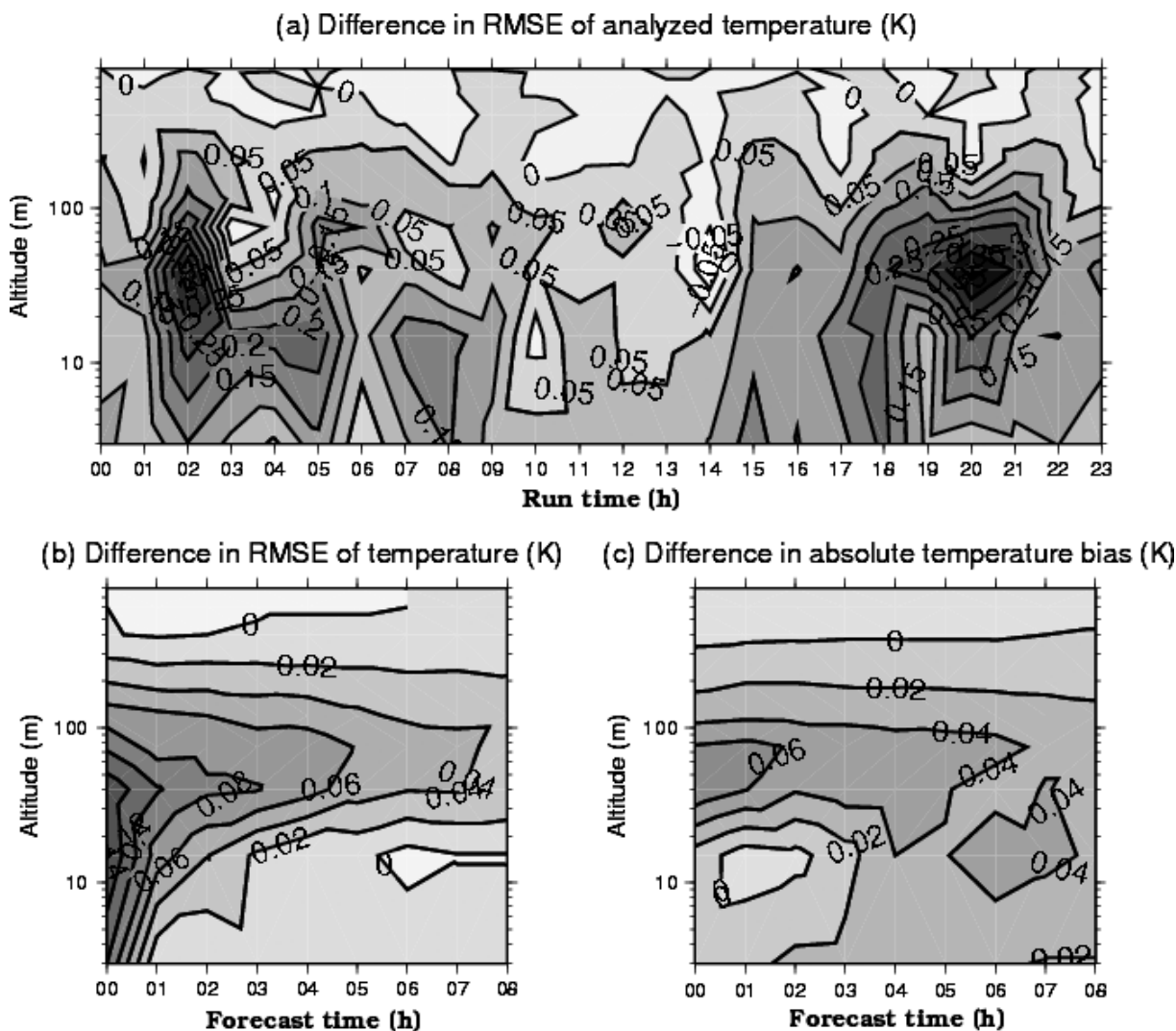


Figure 4. NEAR-FOG, same as Figure 3 for the NOMAST experiment.

### 3.7. Case study

In this subsection, two simulations, starting at day 2 at 0500 and 1100 UTC, are investigated in more detail. Figure 6 shows various temperature profiles: the ‘truth’, the simulated observations and the REF, MAST10 and NOMAST experiments. The ‘truth’ shows that for the simulation starting at 0500 UTC the atmosphere was characterized by a strongly stable stratification, while a slightly unstable stratification characterized the simulation starting at 1100 UTC.

For the simulation starting at 0500 UTC, the ‘observed’ temperature from ALADIN was colder than the ‘truth’ at 20 m and warmer at 50 m. The REF analysis (Figure 6(a)) stayed close to the observations taken in the first 30 m. For the MAST10 analysis, the low ALADIN value at 20 m did not affect the temperature profile, as the 10 m observation from the mast had a much greater weight. However, the warm 50 m ALADIN value had a significant impact on the temperature profile above 20 m, which was about 0.5 K higher than the REF analysis. The lack of the 30 m mast observation increased the proportional weight of the 50 m temperature given by ALADIN, which

led to an increased error in the lower part of the domain. The same phenomenon appeared in the NOMAST experiment: the temperature from ALADIN had a stronger impact on the analysis compared with REF. Both warm (for NOMAST) and cold (for MAST10) bias of the analysis were conserved during the first hour of simulation (Figure 6(b)), which shows that in stable situations the temperature analysis has a large impact on the temperature forecast during the first hours of simulation.

For the simulation starting at 1100 UTC, the NOMAST and MAST10 experiments showed very similar initial temperature profiles (Figure 6(c)). For both NOMAST and MAST10, it was the lack of the 30 m mast observation, colder than the ‘truth’, that resulted in both profiles being warmer than the REF experiment. However, after one hour of simulation (Figure 6(d)), the differences between REF, NOMAST and MAST10 became negligible. This shows that the initial conditions for temperature have much less weight on the forecast for unstable or neutral than for stable boundary layers. The mast observations have an influence on the temperature analysis but not on the forecast temperature: for unstable atmospheres

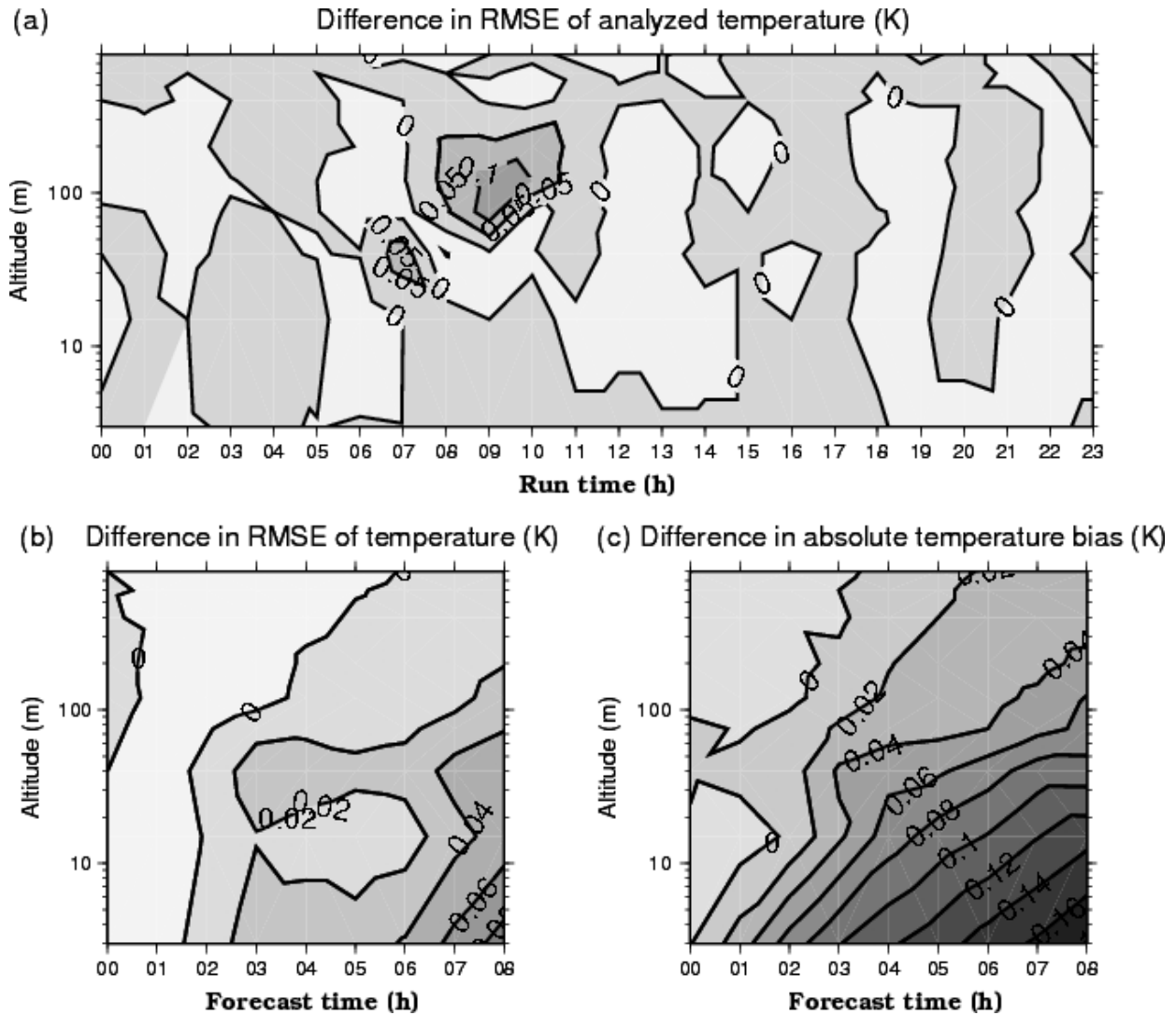


Figure 5. NEAR-FOG, same as Figure 3 for the NOSOIL experiment.

it seems that a 2 m temperature observation is sufficient to adjust the first guess towards the actual state of the boundary layer.

**4. Fog situation**

4.1. Presentation of the situation

This section aims to study the fog and low-cloud life cycle. Fog and low clouds occurred during many nights of the 15 day observation set, hereafter referred to as FOG, because of high moisture combined with strong night-time cooling due to clear skies above the model column. Figure 7 shows the ‘true’ temperature observations at 1 m and the ‘true’ liquid-water content integrated over the model column. In total, 98 hours of LVP conditions were ‘observed’ in these 15 days, with fog occurrence on 11 nights. Stratus also occurred in the upper part of the model column on days 7 and 8, which were not counted as LVP. Various fog situations occurred, from shallow early-morning fog to fog layers more than 200 m thick.

We are going to study the same three scenarios as for the NEAR-FOG situation (MAST10, NOMAST and NOSOIL), plus three additional ones, as follows.

- NORAD: simulations using no radiative flux observations. The height of the fog-layer top is then arbitrarily fixed at 25 m above the ground.
- SODAR: simulations using the reference observation system and simulated sodar observations that provide the height of the cloud-layer top. Here, the above-mentioned minimization algorithm used the observations of radiative fluxes to estimate the

Table I. Number of simulations falling into the error intervals (in minutes) for the prediction of the onset of fog events during NEAR-FOG.

	[0,15]	[15,45]	[45,90]	>90
REF	17	14	5	8
MAST10	12	14	10	7
NOMAST	14	12	8	6
NOSOIL	16	16	6	9

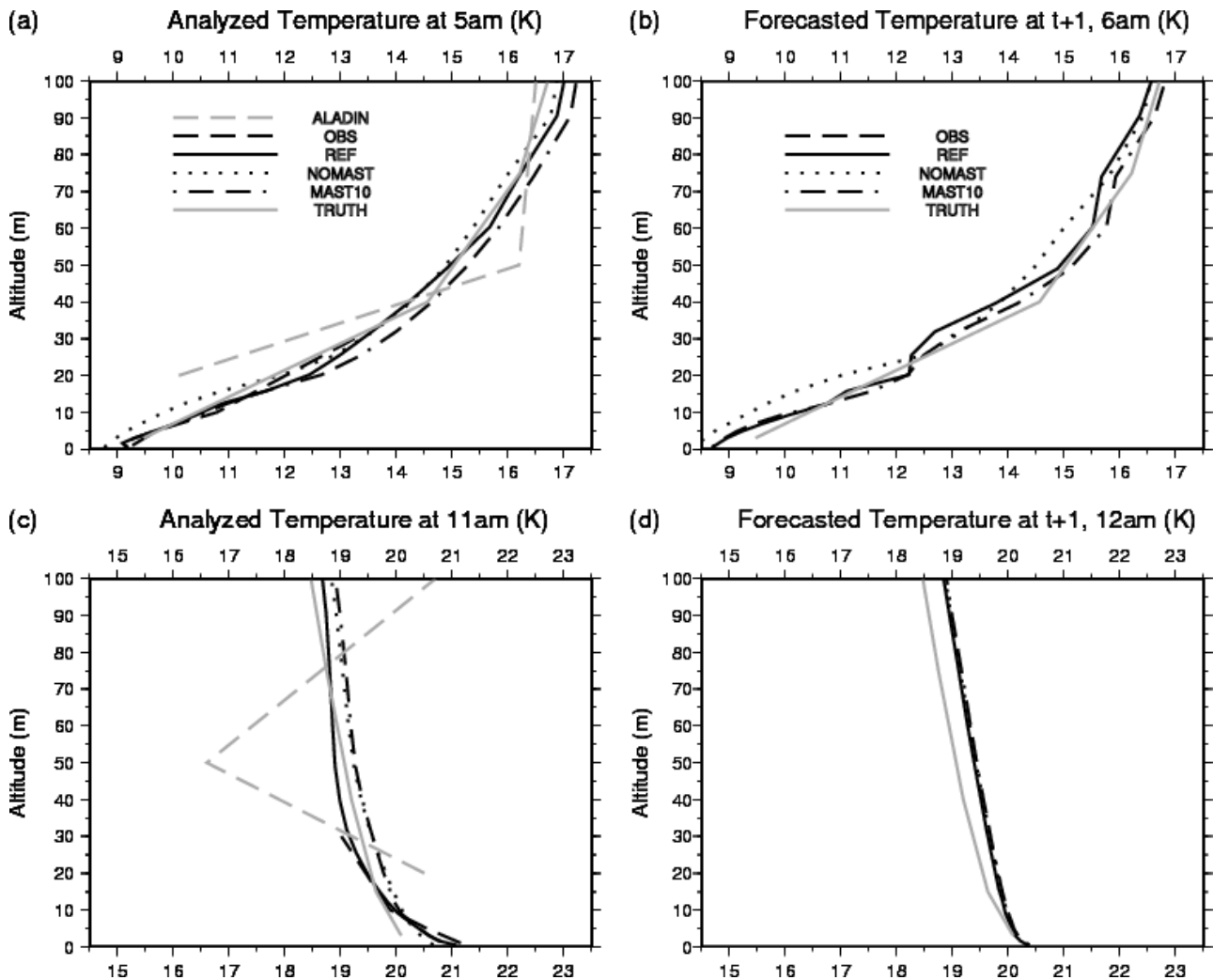


Figure 6. NEAR-FOG, temperature profiles: (a) and (c) temperature at initialization time; (b) and (d) temperature after one hour of simulation, for simulations starting at day 2, 0500 and 1100 UTC. Observations, truth, ALADIN profiles, and experiments REF, NOMAST and MAST10 are plotted.

initial liquid-water content of the cloud. In this case, the radiation scheme was run with the initial cloud thickness as provided by the sodar and with different values for the initial liquid-water content. The best estimate of the initial liquid-water content was the one that minimized the error between the modelled and observed radiative fluxes.

- SODAR\_NORAD: the simulated observations from a sodar provided the height of the cloud-layer top. The initial mixing ratio of liquid water within the cloud layer was arbitrarily fixed at 0.2 g/kg. In this case, the radiative flux observations were not used. Observations during fog events (Duykerke, 1991; Wendish *et al.*, 1998; Colomb and Tzanos, 2005) give values ranging from 0.05–0.5 g/kg. The value we chose lay roughly in the middle of this range. Simulations were carried out with different initial values for the liquid-water mixing ratio, without revealing a significant difference. The same value for the initial mixing ratio of liquid water was used for all the other experiments with the exception of SODAR.

The FOG situation had more LVP situations than the NEAR-FOG (98 hours against 21 hours), so we shall assess the model performance in terms of LVP forecast, in addition to the scores on analyzed and forecast temperature. This assessment will be reported in a separate subsection.

The MAST10 and NOMAST experiments showed the same patterns for FOG and NEAR-FOG in terms of temperature and specific humidity. There was a marked difference between FOG and NEAR-FOG for the NOSOIL experiment, which will be commented on below.

#### 4.2. Simulations with a reference observation system: REF

The reference observation system used for these simulations was the one used at Paris–Charles De Gaulle airport. Figure 8 shows the RMSE and bias of temperature when the reference observation system was used. It is interesting to compare it with Figure 2. The RMSE of the analyzed temperature is in the same range for both situations, except for errors due to the initialization of the

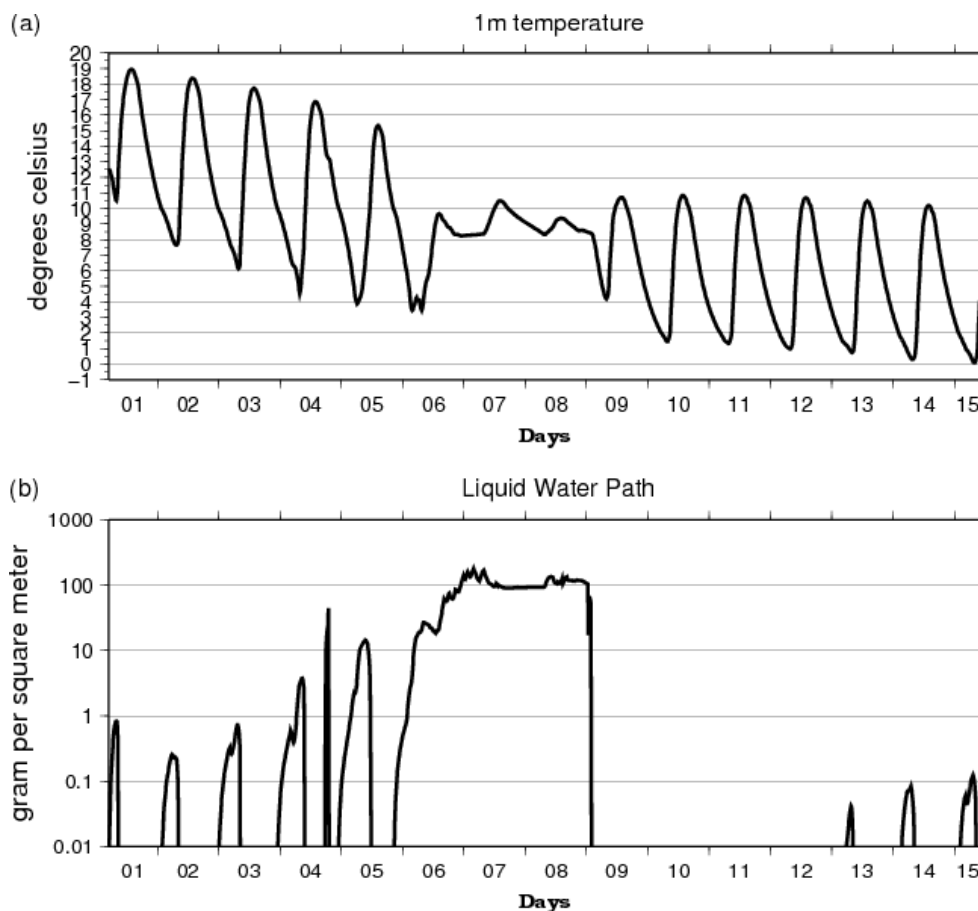


Figure 7. Same as Figure 1 for FOG.

fog-layer thickness, which deteriorate the RMSE of analyzed temperature between 0700 and 1100 UTC, in the 70–100 m altitude range. The RMSE of forecast temperature increases much faster in the lower part of the domain for FOG (Figure 8(b)) than for NEAR-FOG (Figure 2(b)) and reaches a maximum of 1 K after seven hours of simulation. Above 100 m, the RMSE shows small fluctuations around the 0.5 K range. A maximum appears between 40 and 70 m of altitude, which corresponds to situations where the forecast height of the fog is different from the observations. The inversion at the top of the fog layer significantly increases the error if the forecast cloud-layer thickness is not the same as the observed one. The bias also increases with forecast time, but to a lesser extent than for the NEAR-FOG situation, especially above 50 m.

#### 4.3. Simulations with no soil temperature and water content observations: NOSOIL

As mentioned above, the results of this section could vary greatly depending on which land-surface scheme was used. The RMSE of analyzed temperature (not shown) showed little difference from the REF experiment, which was the same as NOSOIL with NEAR-FOG. However, the degradation in both the RMSE and the bias of forecast temperature with forecast time was much greater in the FOG experiment than in NEAR-FOG. In both cases the

degradation was driven by the ground and affected the whole domain after 4–5 h of forecast time. The RMSE was degraded by up to 0.2 K close to the ground after seven hours of forecast and the bias by 0.25 K. As noted in the NEAR-FOG experiment, a higher soil water-content value was the leading factor for this cold bias. In contrast to the NOSOIL experiment with the NEAR-FOG situation, the slower warming rate during daytime due to the above-mentioned factor was much more important than the less intense night-time cooling. The difference from NEAR-FOG may be explained by the fact that fog and low-cloud occurrence, which inhibits both night-time cooling and daytime warming, is much more frequent for FOG than for NEAR-FOG. Also, for FOG, fog and low cloud occur more often during the nights than during the days. During foggy or cloudy situations, the impact of the error of the soil water content is reduced and, since such a situation is more frequent at night, the daytime warming is more affected by this error than the night-time cooling for the FOG situation.

#### 4.4. Simulations with no observations of radiative fluxes: NORAD

In the reference system, radiative flux observations at 2 and 45 m were used to estimate the initial thickness of the fog layer (see Bergot *et al.* (2005) for more detail).

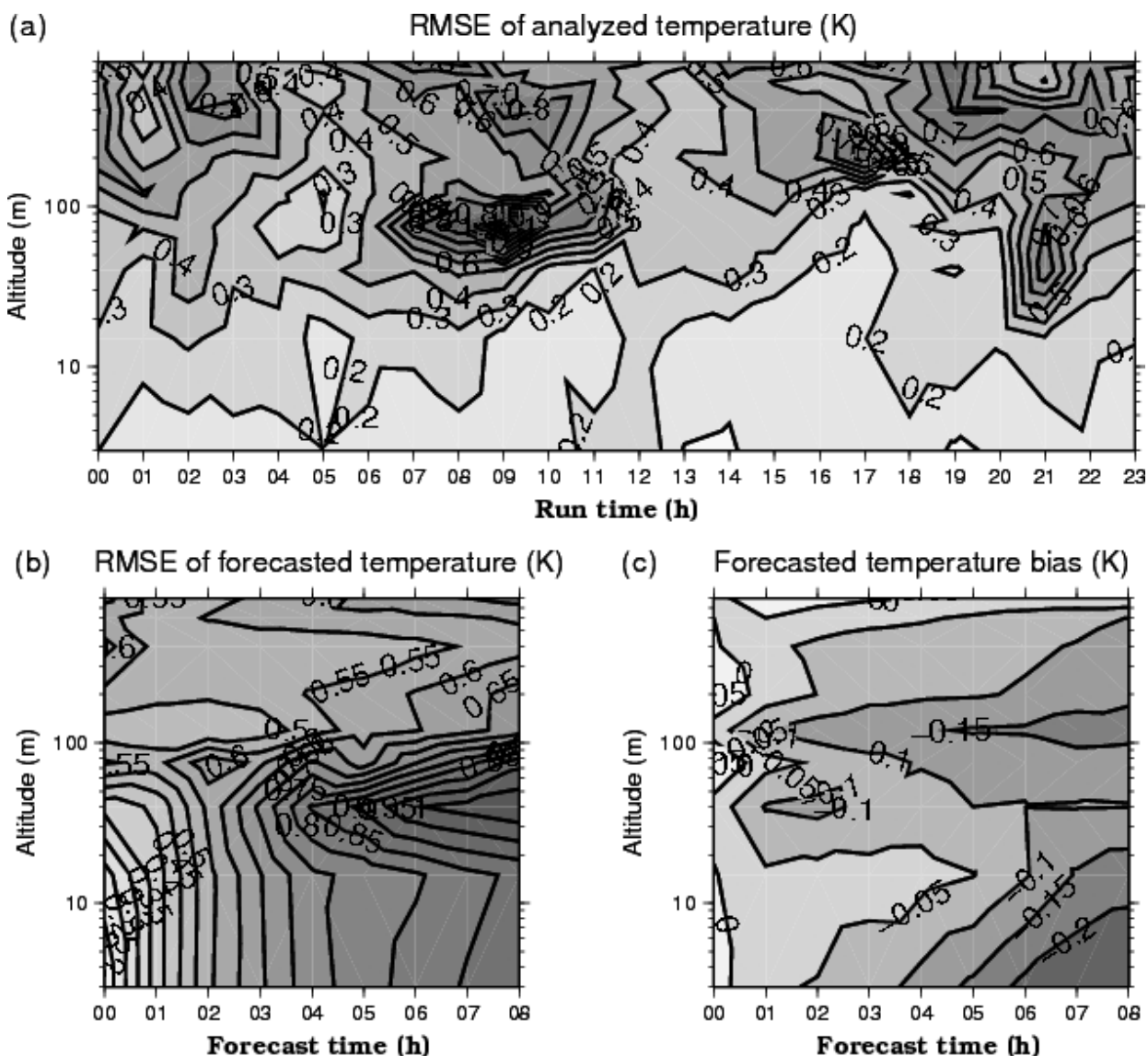


Figure 8. Same as Figure 2 for FOG.

In this experiment (called NORAD), the thickness of the fog/stratus layer was arbitrarily fixed at 25 m.

The RMSE difference for analyzed temperature profiles (Figure 9(a)) was large at the times and altitudes relevant in fog events. The degradation was very marked for the situations where fog was observed, because the inversion at the top of the fog layer was initialized at the wrong altitude. The domain affected by these errors is clearly visible in Figure 9(a) and extends between 0000 and 1400 UTC for simulation times and 30 and 200 m for altitude. The same phenomenon was noted for specific humidity (not shown).

The RMSE difference of forecast temperature (Figure 9(b)) between REF and NORAD soon became large with forecast time. After two hours of forecast, the maximum was reached for altitudes below 20 m. The RMSE was then nearly twice that of the REF experiment. Above 300 m, the degradation was small, as clear skies were frequent. The marked degradation of the RMSE below 300 m can be explained by the fact that the occurrence

or non-occurrence of fog or stratus in the forecasts has a great influence on temperature in and under the cloud layer, as well as just above it, in the inversion layer. The thickness of the initial fog layer partly determines the forecast lift-off time, and thus has a great impact on the scores of forecast temperature, though not on analyzed temperature.

Associated with this RMSE increase is a rise of the forecast temperature absolute bias (Figure 9(c)). Both the RMSE and absolute bias difference follow the same pattern, linked with the evolution of the forecast cloud layer. In an operational configuration, the real fog thickness is, obviously, not known, yet a strong negative (or positive) bias of forecast temperature can be the signature, among other things, of an overestimated (or underestimated) initial thickness of the cloud layer.

Simulations were also run with other figures for the initial fog thickness: 10, 15 and 40 m. The conclusions are mainly the same.

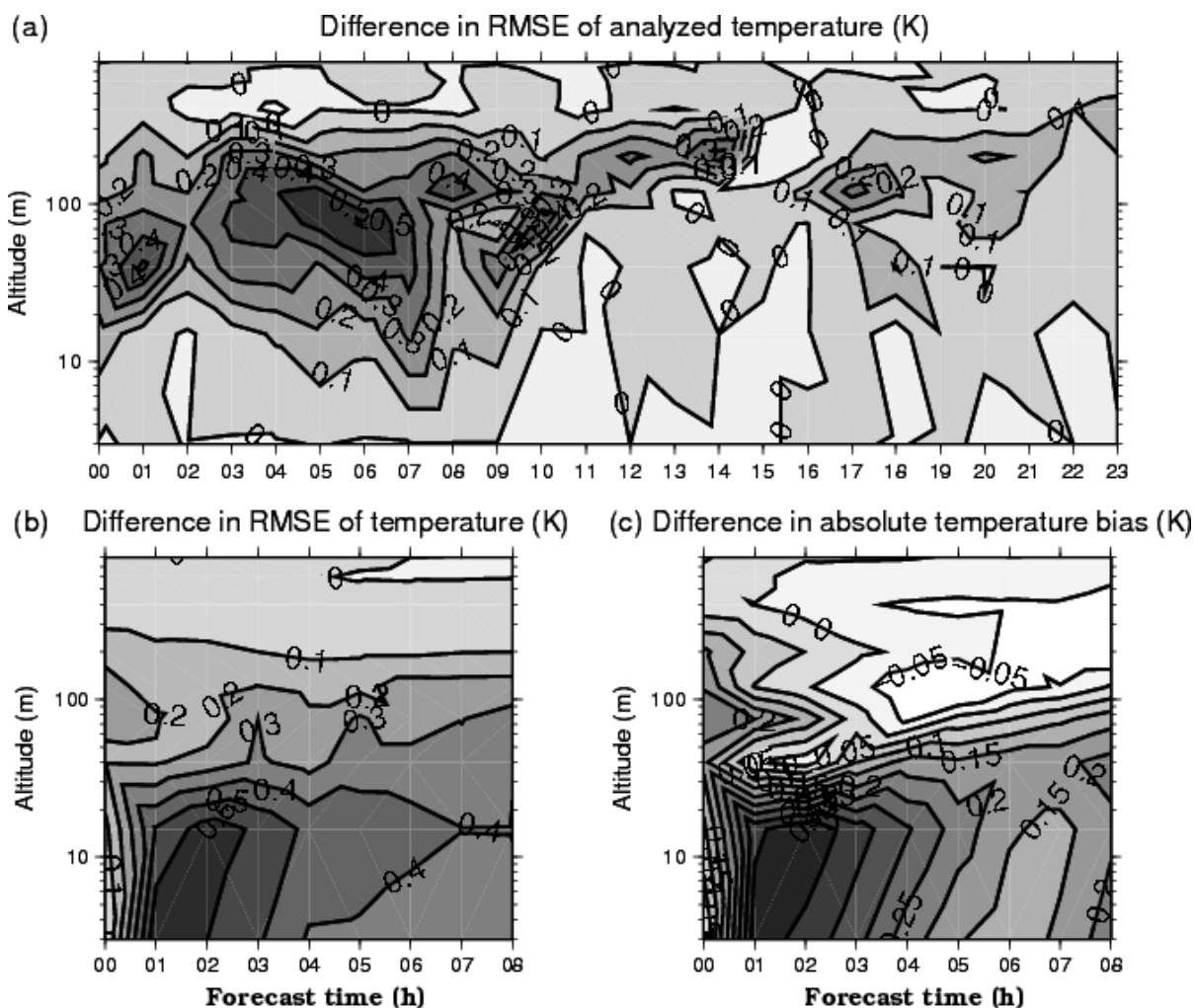


Figure 9. FOG, same as Figure 3 for the NORAD experiment.

4.5. Simulations with addition of a sodar: SODAR and SODAR\_NORAD

The RMSE of the analyzed and forecast temperature, as well as the temperature bias (not shown), were unchanged for the SODAR experiment, compared with REF. That can be explained by the fact that determining the thickness of the cloud layer using the observations from the sodar and then minimizing the error in the radiative fluxes against observations to estimate the liquid-water content of the cloud layer is equivalent to minimizing the optical-thickness error as carried out in the REF experiment.

Both the RMSE of the analyzed and forecast temperature and the temperature bias (not shown) were only slightly degraded for the SODAR\_NORAD experiment compared with the REF experiment, and conclusions similar to those for the SODAR experiment were drawn.

4.6. Influence of the observation system on the fog forecasts

In this subsection, an evaluation of the various experiments will be made in terms of LVP forecasts. We evaluated the skill of the forecast system by comparing the

Hit Rate (HR) and the pseudo-false alarm ratio (pseudo-FAR) of LVP events. In the case of rare event forecasting, such as fog and LVP conditions, the pseudo-FAR is convenient because it removes the impact of the ‘no-no good forecasts’ (no LVP forecast and no LVP observed), which mostly dominate the data sample and hide the true skill of the LVP forecast system.

If we take *a* as the number of observed and forecast events, *b* as the number of not observed and forecast events, and *c* the number of observed and not forecast events, HR and pseudo-FAR are then defined as follows.

$$HR = \frac{a}{a + c}; \quad \text{pseudoFAR} = \frac{b}{a + b}.$$

Table II shows the mean of the HR and pseudo-FAR for all simulations and forecast times. These scores are much more satisfactory than the ones obtained when using real observations (see later tables for a comparison). REF, NOMAST and MAST10 have similar HR and pseudo-FAR. For this situation, the influence of the observations from the mast on the forecast of temperature and humidity was too small to have an impact on the scores of the fog forecasts. The NOSOIL and NORAD experiments, however, stand out with a

Table II. Hit rate and pseudo false-alarm rate for LVP conditions over the 15 days of the FOG situation for the REF, MAST10, NOMAST, NORAD, NOSOIL and SODAR experiments, with the mean for all simulations and forecast times.

	HR	Pseudo FAR
REF	0.899	0.077
MAST10	0.910	0.083
NOMAST	0.906	0.073
NOSOIL	0.879	0.098
NORAD	0.859	0.123
SODAR	0.870	0.078
SODAR_NORAD	0.901	0.094

lower HR and a higher pseudo-FAR than the other experiments. For NOSOIL, a large degradation in the temperature-forecast quality had a strong impact on fog forecasts. At the same time, the fixed initial thickness for fog in NORAD greatly influenced the forecasts. The SODAR experiment revealed a deteriorated HR and an unchanged pseudo-FAR compared with REF. This confirms the conclusion drawn above, i.e. that the sodar did contribute information in the FOG situation (compared with the NORAD observation) but that the radiative flux observations used to estimate the initial height of the fog performed better for the FOG situation. SODAR\_NORAD HR gave more satisfactory results than SODAR despite a slight degradation of its pseudo-FAR: in that case, using the radiative-flux observations to estimate the initial liquid-water mixing ratio did not improve the fog forecasts much.

Tables III and IV show the error of the predicted time of the onset and burn-off of LVP events. Simulations in which fog is already present at the initialization time were discarded for the computation of the onset scores. For these simulations, it was meaningless to compare the simulated and observed onset times because the fog events considered had begun before the initialization time. For the onset time prediction, NOMAST and MAST10 showed a slight degradation compared with REF, while NOSOIL caused fewer large errors (greater than 90 min) than REF, because of less intense night-time cooling for this experiment, as mentioned above. NORAD, SODAR and SODAR\_NORAD all show scores in the same range as REF. As for the burn-off time, the errors were generally smaller than for the onset time. MAST10 and NOMAST were a little less accurate than REF but nevertheless they led to fewer large errors. NOSOIL and NORAD (the latter in particular) significantly deteriorated the forecast of burn-off time, which was consistent with the conclusions drawn above. SODAR, causing more frequent large errors, is slightly worse than REF, and SODAR\_NORAD further deteriorates the prediction of the burn-off time of LVP conditions.

To conclude for the FOG situation, while most observations do not alter fog forecasts scores much (even though they have an impact on the RMSE of analyzed and forecast temperature), it seems that the observations that help

Table III. Same as Table I for FOG.

	[0,15]	[15,45]	[45,90]	>90
REF	29	23	15	18
MAST10	24	27	11	20
NOMAST	27	20	16	16
NOSOIL	28	19	17	11
NORAD	29	23	10	19
SODAR	29	22	12	22
SODAR_NORAD	29	22	11	17

Table IV. Same as Table III for the prediction of burn-off time.

	[0, 15]	[15, 45]	[45, 90]	>90
REF	47	9	5	21
MAST10	45	12	2	14
NOMAST	43	13	5	16
NOSOIL	32	14	5	19
NORAD	22	16	12	38
SODAR	43	12	6	26
SODAR_NORAD	36	12	9	24

to estimate the thickness of the fog at the initialization time are critical for an accurate forecast of the fog life cycle. Also, soil observations, especially those of water content, play an important role in making more accurate forecasts.

#### 4.7. Focus on the analyzed and forecast optical thickness of the fog

The various experiments have shown the importance of the initialization of fog or low-cloud thickness. However, this is made difficult by the fact that in reality observations are often limited or not available at all. Various algorithms have been used to estimate fog initial optical thickness in the REF, NORAD, SODAR and SODAR\_NORAD experiments and our objective now is to compare and assess them against the 'true' values, which are accessible to us thanks to the OSSE framework. First, we are going to assess the efficiency of the algorithm used in the REF experiment to estimate the fog-layer thickness at the initialization time.

Figure 10 shows the observed and analyzed altitude (above the ground) of the top of the cloud layer for the 15 days of the FOG case. The plotted experiment is REF, which employs radiative flux observations at 2 and 45 m to estimate cloud thickness at the initialization time, if any is present. As discussed above, we arbitrarily chose a value of 0.2 g/kg for the initial liquid-water mixing ratio in the cloud. Simulations with other values gave very similar results. The thickness of the cloud layer at the initialization time was underestimated most of the time. However, even when the right thickness was used, such as in the SODAR and SODAR\_NORAD experiments, the forecast quality was still not improved. Except for the thick fog on days 5 and 6, the fog was relatively

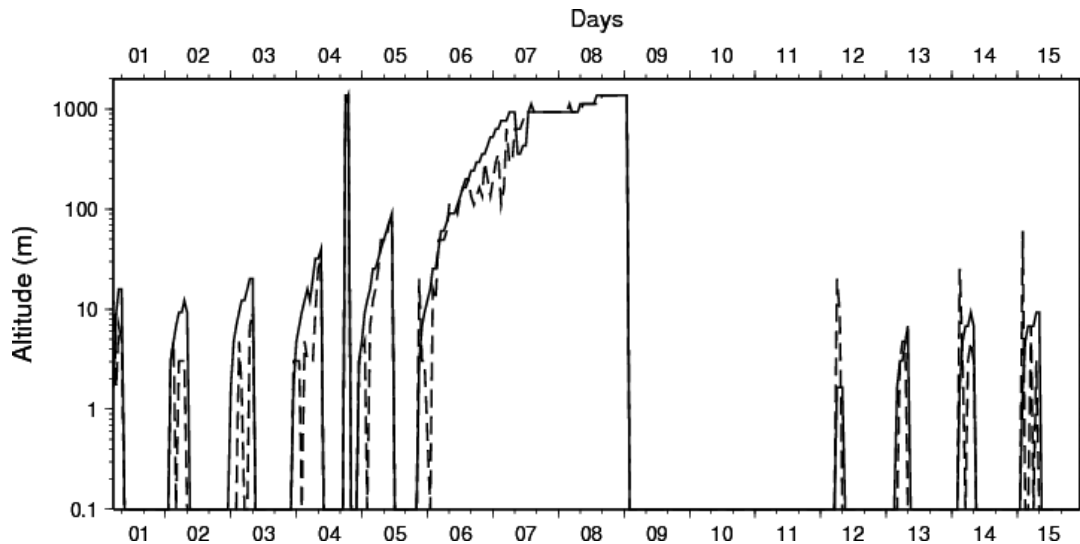


Figure 10. Height of cloud-layer top, as observed (continuous line) and analyzed in the REF experiment (dashed line) for the FOG situation.

shallow and the 'observed' liquid-water mixing ratio was well below 0.2 g/kg. This explains why, although the thickness of the cloud layer at the initialization time was often underestimated, its optical thickness is rather well analyzed most of the time.

We will now look into the impacts of the initialization of fog optical thickness on the forecast of the cloud-layer life cycle, for a simulation starting at day 6, 0600 UTC. A 60 m thick fog was observed then, which lifted from the ground at around 1200 UTC and remained as stratus until the end of the simulation. Since our objective was to assess the influence of the initial optical thickness of the fog only, all other variables at the initialization time remained the same for all experiments (the values of the REF experiment were used). The TRUTH experiment is the simulation using these initial conditions and the 'true' values for liquid-water content at the initialization time. In addition, only experiments that had a direct impact on the thickness or on the liquid-water content of the fog at the initialization time were run: REF, NORAD, SODAR and SODAR\_NORAD. Another version of the SODAR\_NORAD experiment, SODAR\_NORAD\_60, was also carried out, with a higher initial optical thickness of the fog, using the initial value of liquid-water content at 0.6 g/kg in the fog layer. The NORAD\_110 experiment was also run with 110 m initial thickness for the fog layer.

Figure 11 shows the analyzed and forecast liquid-water content of the simulation starting at day 6, 0600 UTC, for the TRUTH, REF, NORAD, SODAR, SODAR\_NORAD\_60 and NORAD\_110 experiments. It also shows the liquid-water path for all these simulations. The REF, NORAD and SODAR experiments underestimated the initial liquid-water path of the fog while SODAR\_NORAD\_60 and NORAD\_110 overestimated it.

The REF and NORAD experiment underestimated both the initial fog thickness and its liquid-water content. Microphysical processes such as condensation compensated for this in terms of liquid-water path after one hour of forecast time for REF and two hours for NORAD. Total

evaporation of the cloud occurred half an hour too early for NORAD and fifteen minutes too early for REF. The vertical development of the cloud was the same for REF and TRUTH (130 m), and slightly smaller for NORAD (110 m), while the liquid-water content at the top of the cloud lay within the same range for the three experiments after the adjustment time. This shows that in this situation the model was able to recover from an underestimated initial optical thickness of the cloud. The adjustment time varied depending on the magnitude of the initial error. For shallower fog situations, on the other hand, an underestimation of the initial optical thickness could prove more crucial, as dissipation could occur before the end of the adjustment time. The SODAR experiments showed that, once the initial fog thickness was known, the algorithm used to estimate the liquid-water content underestimated its value compared with TRUTH. The same algorithm also estimated the thickness of the fog layer for REF, which typically led to the aforementioned underestimated values.

In the case of SODAR\_NORAD\_60, microphysical processes quickly reduced the liquid-water content of the cloud, and in less than fifteen minutes of simulation the maximum liquid-water content at the top of the fog layer fell within the same range as TRUTH, i.e. 0.4 g/kg. The optical thickness of the cloud was then very similar to TRUTH, with a total evaporation of the cloud occurring at the same time. For the NORAD\_110 experiment, the initial optical thickness of the cloud was only slightly greater than TRUTH. This was because the underestimation of the initial liquid-water content partially offset the overestimation of the initial thickness of the cloud. The same microphysical processes as noted in NORAD quickly brought the maximum liquid-water content into the same range as TRUTH, which resulted in a large overestimation of the optical thickness of the cloud throughout the forecast. The vertical development of the cloud was greater than in the TRUTH experiment (160 m against 130 m) and the cloud was still very

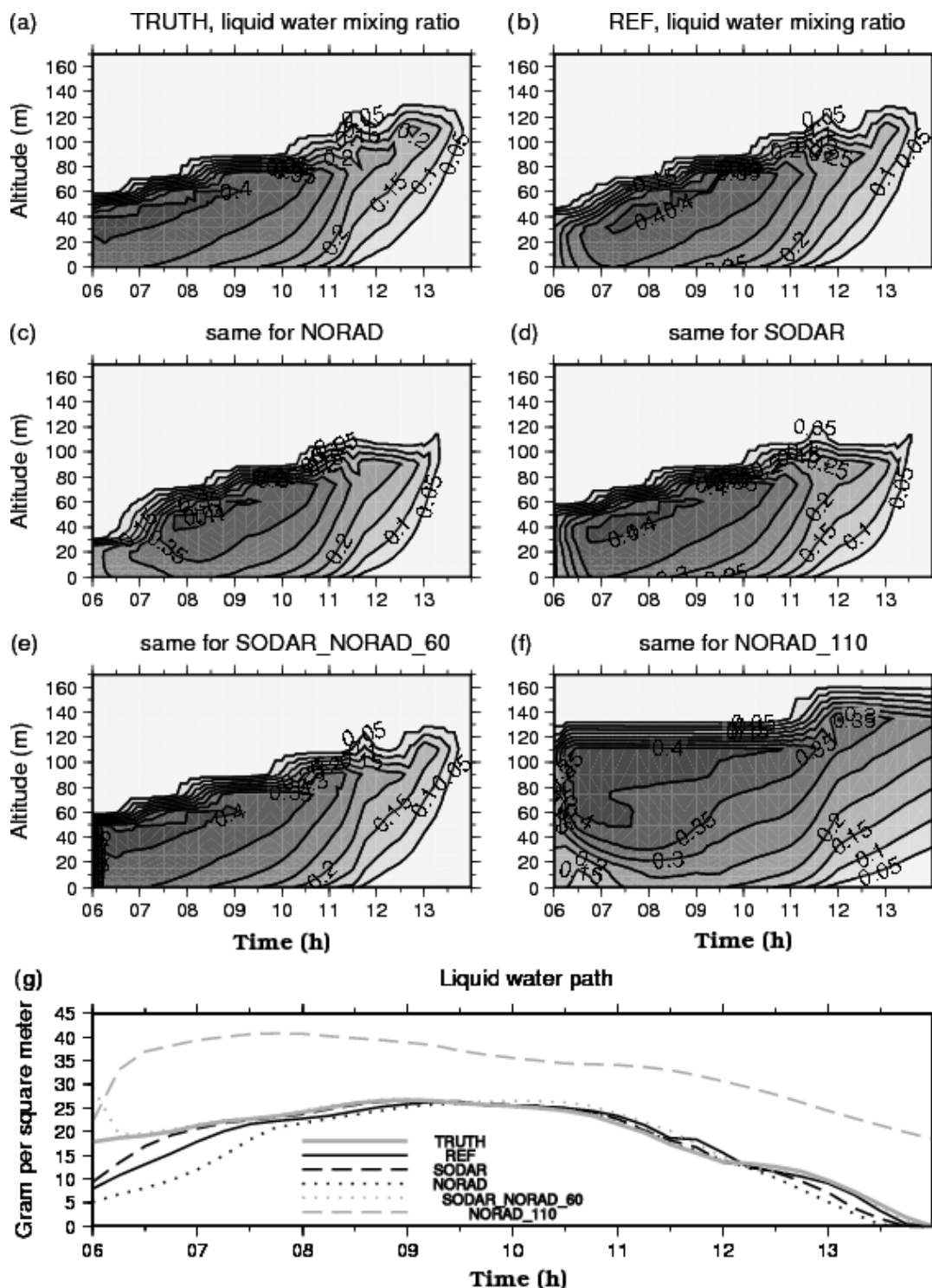


Figure 11. Simulation starting at day 6, 0600 UTC, liquid-water versus time for (a) TRUTH, (b) REF, (c) NORAD, (d) SODAR, (e) SODAR\_NORAD\_60, (f) SODAR\_NORAD\_110; and liquid-water path of each of these experiments (g).

thick at the time, corresponding to its dissipation in TRUTH.

To conclude, it seems that for this simulation the initial thickness of the fog is in fact more important than the initial optical thickness. The model is also more sensitive to an overestimation, rather than an underestimation, of the initial fog thickness. This explains why the algorithm that estimates the initial fog thickness using radiative

flux observations works well, since it results in an underestimation of this thickness most of the time.

### 5. Study using real observations

In this section, experiments are reported that used real observations from Paris–Charles de Gaulle airport, over the winter of 2004–2005. For this situation (referred to

as REAL), we performed the same experiments as in NEAR-FOG and FOG, i.e. the reference experiment REF, MAST10, NOMAST, NORAD and NOSOIL. Observations from a sodar were not available in this case, so there were no SODAR or SODAR\_NORAD experiments.

The test period covered November and December 2004 and January 2005, with hourly simulations, which represents around 2200 eight-hour simulations. 168 hours of LVP conditions were observed during these months. Fog and low-cloud conditions were more frequent late at night and early in the morning and were less frequent during the afternoons.

### 5.1. LVP conditions forecast

Tables V and VI display the mean hit ratio (HR) and pseudo false-alarm ratio (FAR) of LVP conditions, for various forecast times, for the REAL case. MAST10 had HR and FAR nearly identical to those of REF while NOMAST was slightly deteriorated, especially for the HR. The NOSOIL experiment showed significant increases in both HR and FAR, implying an underestimation of the prescribed soil water content, which led to stronger cooling at night. Finally, the NORAD experiment showed a sharp decrease of HR. This was partly due to premature fog burn-offs because the initial thickness of the cloud layer was underestimated.

The overall conclusions using real observations are qualitatively close to those obtained with simulated observations: the most crucial observations are the ones that help initialize the thickness of the fog, followed by soil water measurements and mast observations. With both simulated and real observations, it seems that observations from a 10 m mast give the same results as those from a 30 m mast for the LVP forecast.

Table V. Hit ratio (HR) of LVP conditions for various forecast times for the REAL situation and for the 1 November 2004–31 January 2005 period.

	[0–3 h]	[3–6 h]	[6–8 h]	all
REF	0.72	0.56	0.47	0.62
MAST10	0.73	0.56	0.46	0.62
NOMAST	0.72	0.55	0.45	0.61
NOSOIL	0.81	0.73	0.62	0.75
NORAD	0.63	0.52	0.48	0.57

Table VI. Pseudo false-alarm ratio (FAR) of LVP conditions for various forecast times for the REAL situation and for the 1 November 2004–31 January 2005 period.

	[0–3 h]	[3–6 h]	[6–8 h]	all
REF	0.42	0.53	0.61	0.49
MAST10	0.4	0.52	0.61	0.49
NOMAST	0.44	0.54	0.63	0.51
NOSOIL	0.49	0.62	0.68	0.59
NORAD	0.42	0.53	0.61	0.49

### 5.2. Onset and burn-off of LVP events

Tables VII and VIII show the error of the predicted time of onset and burn-off. Simulations in which fog was present at initialization were discarded for score computation for fog onset, for the same reasons as mentioned before.

For the onset (Table VII), MAST10 did not deteriorate the skill compared with REF. NOMAST showed a greater deterioration, and NOSOIL was less effective than the other experiments, especially for large errors (arbitrarily defined as larger than 360 min for the REAL situation). NORAD had a definite impact on the onset time forecast, without a clear trend except for a slightly increasing frequency of large errors. This shows that modifications of the analysis (in this case only when fog situations or low clouds are present) have an impact on later runs through the sequence of first guesses and analysis. As for the burn-off, large errors were less frequent due to simulations that forecast LVP conditions until the end of the forecast time. Therefore there was no recorded burn-off for such cases. MAST10 and NOMAST did not greatly affect the overall skill of the model in forecasting the LVP burn-off time, but the number of large errors was significantly reduced with NOMAST. On the other hand, their number was greatly increased by NOSOIL, which in turn reduced the skill of the model for the forecast burn-off time. NORAD did not affect the frequency of large errors but deteriorated the burn-off time forecast. In general, the conclusions drawn from simulated observations are also valid with real observations, even though there is a difference in the scale of error.

## 6. Conclusion

Fog is a physical phenomenon that remains particularly difficult to forecast. In order to render a 1D approach useful, local observations will have to be used to initialize temperature and humidity correctly. More or less extensive local observation systems were tested with the assimilation scheme of COBEL–ISBA, first with simulated observations and then with real observations. This study demonstrates that the most crucial observations for accurately initializing and forecasting fog situations are the ones that provide an estimation of the initial height of the cloud. They have a strong impact on the forecast of the fog burn-off time, and also on the onset time forecast in the case of recurrent fog, such as in the FOG situation. Soil water-content measurements are also important for an accurate forecast in terms of both onset and burn-off times. A measurement mast significantly improves the initial temperature and humidity profiles, an improvement that is propagated in the forecast, especially during the night. However, it has been shown that using a 10 m mast instead of a 30 m one does not deteriorate the forecast of fog events as such.

This study is based on one single model and the results are therefore likely to be model-dependant, for both the atmospheric model (COBEL) and the land-surface scheme (ISBA). Nevertheless, it underlines the

Table VII. Same as Table I for REAL.

	[0,15]	[15,45]	[45,90]	[90,180]	[180,240]	[240,360]	>360
REF	18	16	18	28	16	16	72
MAST10	24	14	18	22	14	20	70
NOMAST	16	16	24	24	16	18	72
NOSOIL	28	26	32	18	14	28	176
NORAD	28	18	20	20	16	24	76

Table VIII. Same as Table IV for REAL.

	[0,15]	[15,45]	[45,90]	[90,180]	[180,240]	[240,360]	>360
REF	50	16	28	20	12	16	40
MAST10	40	32	24	22	8	12	36
NOMAST	48	26	24	26	14	12	30
NOSOIL	44	10	18	18	12	20	66
NORAD	52	38	14	32	2	18	38

importance of an accurate initialization of fog and low clouds and of the soil-atmosphere interface. These general conclusions can also be helpful for 3D simulations of radiation fog.

We should bear in mind that simulated observations are a very different framework from real observations. The fact that model error is avoided allows a better understanding of the sources of error at initialization and of the relations between the initial and forecast profiles. Having compared the scores of the FOG and REAL experiments for the fog onset and burn-off time error, it is clear that model errors are significant, leading to delayed forecasts for both the onset and burn-off time. However, the conclusions drawn with simulated observations concerning the observation system are qualitatively the same for simulated and real observations.

These insights into the impact of observations on the analysis and the forecasting of fog events will help to define the appropriate initialization scheme for fog forecasting. The case study has shown a sharp difference of model behaviour during the daytime and night-time. The correlation between the forecast values of temperature and humidity at lower and higher levels also follows a diurnal cycle. The assimilation scheme should thus take into account the variability of atmospheric conditions and their impact on the performance of the model and the background-error variances and covariances. This can be achieved by means of an ensemble Kalman filter (EnKF), as shown by Hacker and Snyder (2005) and Hacker and Rostkier-Edelstein (2007). The adaptation of the EnKF approach to 1D fog modelling is the subject of ongoing efforts.

### Acknowledgements

We wish to thank three anonymous reviewers as well as the Editor and the Associate Editor for their valuable comments and suggestions, which improved the

manuscript. We are also grateful to Robert Tardif for his comments.

### References

- Bergot T, Guédalia D. 1994a. Numerical forecasting of radiation fog. Part I: Numerical model and sensitivity tests. *Mon. Weather Rev.* **122**: 1218–1230. DOI: 10.1175/1520-0493(1994)122<1218:NFORFP>2.0.CO;2.
- Bergot T, Guédalia D. 1994b. Numerical forecasting of radiation fog. Part II: A comparison of model simulation with several observed fog events. *Mon. Weather Rev.* **122**: 1231–1246. DOI: 10.1175/1520-0493(1994)122<1231:NFORFP>2.0.CO;2.
- Bergot T, Carrer D, Noilhan J, Bougeault P. 2005. Improved site-specific numerical prediction of fog and low clouds: a feasibility study. *Weather and Forecasting* **20**: 627–646. DOI: 10.1175/WAF873.1.
- Bergot T, Terradellas E, Cuxart J, Mira A, Liechti O, Müller MD, Nielsen NW. 2006. Intercomparison of single-column numerical models for the prediction of radiation fog. *J. Appl. Meteorol. Climatol.* **46**: 504–521. DOI: 10.1175/JAM2475.1.
- Capon R, Tang Y, Clark P. 2007. A 3D high resolution model for local fog prediction. *NetFAM/COST 722 workshop on cloudy boundary layer, Toulouse, France*. <http://netfam.fmi.fi/CBL07/capon.pdf> [Accessed August 2008].
- Chen F, Janjic Z, Mitchell K. 1997. Impact of atmospheric surface-layer parametrizations in the new land-surface scheme of the NCEP mesoscale eta model. *Boundary-Layer Meteorol.* **85**: 391–421.
- Cheung TK. 1991. Sodar observations of the stable atmospheric boundary layer at Barrow, Alaska. *Boundary-Layer Meteorol.* **57**: 251–274. DOI: 10.1007/BF00120887.
- Clark DA. 2002. The 2001 demonstration of automated cloud forecast guidance products for San-Francisco international airport. *Proc. 10th Conf. on Aviation, Range, and Aerospace Meteorology, AMS*. [http://www.ll.mit.edu/mission/aviation/publications/publication-files/ms-papers/Clark\\_2002\\_ARAM\\_MS-15290\\_WW-10474.pdf](http://www.ll.mit.edu/mission/aviation/publications/publication-files/ms-papers/Clark_2002_ARAM_MS-15290_WW-10474.pdf) [Accessed August 2008].
- Clark DA. 2006. Terminal ceiling and visibility product development for northeast airports. *Proc. 14th Conf. on Aviation, Range, and Aerospace Meteorology, AMS*. <http://jobfunctions.bnet.com/abstract.aspx?docid=321609> [Accessed August 2008].
- Colomb M, Tzanos D. 2005. Microphysical data of fog observed in Clermont-Ferrand and corresponding satellite images. *Second Midterm Workshop on short range forecasting methods of fog, visibility and low clouds, 2005*. [http://lcrs.geographie.uni-marburg.de/fileadmin/COST\\_media/Official\\_documents/Publications/proceedings\\_Langen.pdf](http://lcrs.geographie.uni-marburg.de/fileadmin/COST_media/Official_documents/Publications/proceedings_Langen.pdf) [Accessed August 2008].
- Duynkerke PG. 1991. Radiation fog: a comparison of model simulation with detailed observations. *Mon. Weather Rev.* **119**: 324–341. DOI: 10.1175/1520-0493.

- Foken Th, Albrech H-J, Sasz K, Vogt F. 1997. Operational use of sodar information in nowcasting. In, *Acoustic Remote Sensing Applications, Part Two: Applications in the Atmosphere*, Singal SP (ed.). Springer Verlag: Berlin; Vol. 69, pp 395–405.
- Hacker J, Rostkier-Edelstein D. 2007. PBL state estimation with surface observations, a column model, and an ensemble filter. *Mon. Weather Rev.* **135**: 2958–2972. DOI: 10.1175/MWR3443.1.
- Hacker J, Snyder C. 2005. Ensemble Kalman filter assimilation of fixed screen-height observations in a parametrized PBL. *Mon. Weather Rev.* **133**: 3260–3275. DOI: 10.1175/MWR3022.1.
- Herzogh PH, Benjamin SG, Rasmussen R, Tsui T, Wiener G, Zwack P. 2003. Development of automated analysis and forecast products for adverse ceiling and visibility conditions. *Proc. 19th International Conference on Interactive Information and Processing Systems for Meteorology, Oceanography and Hydrology, AMS*. <http://ams.confex.com/ams/pdfpapers/57911.pdf> [Accessed August 2008].
- Huang XY, Wang H, Chen Y, Zhang X, Tjernkes SA, Stuhlmann R. 2007. An observing system simulation experiment using both MM5 and WRF: experiment configuration and preliminary results. *Presentation at the 8th WRF annual meeting, 2007*. <http://www.mmm.ucar.edu/wrf/users/workshops/WS2007/abstracts/p2-2-Huang.pdf> [Accessed August 2008].
- Müller MD, Masbou M, Bott A, Janjic Z. 2005. Fog prediction in a 3D model with parametrized microphysics. *Proc. WWRP Int. Symp. on Nowcasting and Very Short-Range Forecasting*. **6.26**. [http://www.meteo.fr/cic/wsn05/resumes\\_longs/6.26-96.pdf](http://www.meteo.fr/cic/wsn05/resumes_longs/6.26-96.pdf) [Accessed August 2008].
- Müller MD, Schmutz C, Parlow E. 2007. A one-dimensional ensemble forecast and assimilation system for fog prediction. *Pure Appl. Geophys.* **164**: 1241–1264. DOI: 10.1007/s00024-007-0217-4.
- Roquelaure S, Bergot T. 2008. A local ensemble prediction system (L-EPS) for fog and low clouds: construction, Bayesian model averaging calibration and validation. *J. Appl. Meteorol. Climatol.* **47**: 3072–3088. DOI: 10.1175/2008JAMC1783.1.
- Wendish M, Mertes S, Heintzenberg J, Wiedensohler A, Schell D, Wobrock W, Frank G, Martinsson BG, Fuzzi S, Orsi G, Kos G, Berner A. 1998. Drop size distribution and LWC in Po valley fog. *Contrib. Atmos. Phys.* **71**: 87–100. DOI: 10.1175/2008JAMC1783.1.
- Yushkov VP, Kouznetsova IN. 2008. Comparison of nocturnal inversion characteristics obtained by sodar and microwave temperature profiler. *IOP Conf. Ser.: Earth and Environmental Science*. **1**: 1265–1282. DOI: 10.1088/1755-1315/1/1/012047. [http://www.iop.org/EJ/article/1755-1315/1/1/012047/ees8\\_1\\_012047.pdf](http://www.iop.org/EJ/article/1755-1315/1/1/012047/ees8_1_012047.pdf) [Accessed August 2008].